COMFIS - Comparative Visualization of Simulated Medical Flow Data

M. Meuschke[1], S. Voß[2], P. Eulzer[3], G. Janiga[2], C. Arens[4], R. Wickenhöfer[5], B. Preim[1], K. Lawonn[3]

[1]Department of Simulation and Graphics, University of Magdeburg, Germany
[2]Institute of Fluid Mechanics and Thermodynamics, University of Magdeburg, Germany
[3]Institute of Computer Science, University of Jena, Germany
[4]Department of Otorhinolaryngology, University Hospital Gießen, Germany
[5]Herz-Jesu Krankenhaus Dernbach, Germany

Abstract

Simulations of human blood and airflow are playing an increasing role in personalized medicine. Comparing flow data of different treatment scenarios or before and after an intervention is important to assess treatment options and success. However, existing visualization tools are either designed for the evaluation of a single data set or limit the comparison to a few partial aspects such as scalar fields defined on the vessel wall or internal flow patterns.

Therefore, we present COMFIS, *a system for the comparative visual analysis of two simulated medical flow data sets, e.g. before and after an intervention. We combine various visualization and interaction methods for comparing different aspects of the underlying, often time-dependent data. These include comparative views of different scalar fields defined on the vessel/mucous wall, comparative depictions of the underlying volume data, and comparisons of flow patterns. We evaluated* COMFIS *with CFD engineers and medical experts, who were able to efficiently find interesting data insights that help to assess treatment options.*

CCS Concepts

• **Human-centered computing** → *Visualization;* • **Computing methodologies** → *Computer graphics;*

1. Introduction

Medical flow data have become increasingly important w.r.t. the diagnosis and treatment planning of vascular [DCM*18, EDK*20] and respiratory diseases [JĆS*20]. Therefore, patient-specific information on blood and air flow behavior is needed. In smaller vessels, e.g., cerebral vessels, or air-filled structures, e.g., the larynx, flow information can be simulated based on computational fluid dynamics (CFD). CFD simulations of cerebral blood flow aid in risk assessment of pathological structures, such as cerebral aneurysms [DCM*18] and allow to assess the flow behavior in relation to different therapies, e.g., the use of vascular prostheses [MTXS14]. CFD simulations of nasal airflow contribute to the understanding of physiological and pathologically altered nasal breathing, e.g., effects of obstructions and deformities, and provide decision support for surgical interventions [JĆS*20].

Numerous visualization systems have been developed to analyze medical flow data. However, existing non-commercial tools focus either on the visual analysis of a single data set [NBR*18, KGGP19] or are limited to a specific component, such as the surface mesh [GSK*12, MGB*18] or volume [GTB*10, SLG15]. This makes the comparative analysis of pre- and post-treated data as well as different treatment options laborious. Moreover, commercial tools, such as *Ansys Ensight*, require programming skills to link and synchronize data sets that medical experts usually do not have.

We introduce COMFIS, a visualization system for comparative analysis of simulated medical flow data, such as before and after surgery or treatment options. COMFIS allows an interactive and collaborative exploration of similarities and differences between two selected data sets arranged in a linked side-by-side view. We investigate design decisions in close collaboration with CFD engineers and researching physicians. Rather than introducing new visualization or assessment methods, we describe an integrated system for comparative analysis of all three components of medical flow data: a surface mesh, flow volume, and path lines representing flow patterns.

2. Related Work

Related work comprises the visual analysis of medical flow data including cardiac and cerebral hemodynamics as well as nasal aerodynamics. Oeltze et al. [OJMN*19] provide a comprehensive summary of medical flow visualization techniques by highlighting essential exploration tasks. In this paper, we focus on the *compare data task*.

Comparative visualizations support the analysis of simulated data in multiple ways, e.g., understanding different physical phenomena or conditions, such as experimental or numerical [PP95]. In addition, there are visual analytic systems that linked combinations of statistical diagrams and plot-based depictions to support, e.g., the analysis of electronic health records [GFL*20] or clinical decision-making [MSBM*22]. An important decision in comparative systems

is the arrangement of the visualizations. Gleicher et al. [GAW*11] specifies three generic categories for visual comparison: Juxtaposition (separation), superposition (overlay), and explicit encoding (direct representation of relationships). Later they provide a general strategy how to design comparative visualizations and which issues need to be considered [Gle17].

While in CFD or imaging-focused literature [LAM*12, GBMK07, ALEK15] side-by-side views support the comparison task, more advanced methods are optimized for a specific component of the underlying domain. There are approaches dealing with the visual analysis of flow patterns within the flow volume (discussed in Sec. 2.1) as well as of multiple scalar fields defined on the vessel/mucous wall (discussed in Sec. 2.2). Very few approaches focus on an integrated comparison of the wall and volume domain (see Sec. 2.3). A widely used concept is to combine these scientific visualizations with analytical visualizations, such as scatter plots, scatter plot matrices, or parallel coordinates [MNB*21, RvdHD*15], to investigate, e.g., correlations or temporal behavior of attributes.

2.1. Comparative Visualizations inside the Lumen

The comparative flow analysis inside the vessel lumen or nasal cavity plays an important role to assess treatment success. Domain experts want to see how flow properties comprising both quantitative features, e.g., flow velocity, as well as qualitative features, e.g., inflow jet, behave. Since medical and CFD experts are familiar with side-by-side views, different extensions of this concept exist to simplify the comparison. Oeltze et al. [OLK*14] focused on an improved assessment of treatment options for cerebral aneurysms. They clustered blood flow-representing streamlines before and after the virtual stenting. Similarly, clustering is used to classify flow patterns, e.g., in cerebral aneurysms [MOJB*19] or the aorta [MLK*16].

Another option is to simplify the depiction within side-by-side views by showing a straightened representation of the vasculature. Angelelli et al. [AH11] proposed a straightening of the aorta and internal flow characteristics, where multiple instances are visualized side by side. Behrendt et al. [BPEGP21] introduced a flattened representation of the aorta and path lines, which are transformed into a normalized centerline space to compare different patients.

In addition, perpendicular cut planes are often used to compare flow regions. Lamata et al. [LPK*14] defined several cut planes within the aorta to show the average pressure around the corresponding centerline point. However, quantitative comparisons are challenging due to the usage of absolute distances from the mitral valve as y-axis. Karimkeshteh et al. [KKN*19] overcome this problem by normalizing the aorta between a set of pre-defined anatomical positions along the aorta. Behrendt et al. [BEGP18] calculated differences in flow velocity, direction and flow jet position of two measured aortic blood flow data sets. The results are color-coded on linked cut planes, where the data sets are arranged side by side.

Another option is a 2D color scale applied to integral curves to compare, e.g., different treatment options and their effects on the blood flow [GTB*10]. De Hoon et al. [dHvPJV14] used colored vector glyphs to encode differences in orientation angle between simulated and measured blood flow. Verma and Pang [VP04] presented glyph-based methods to compare streamlines and stream ribbons as

well as a volume rendering to compare dense fields of streamlines. Furthermore, more abstract representations are used to compare flow characteristics between data sets. Meuschke et al. used several glyph-based techniques to encode similarities and differences between cohorts based on measured aortic blood flow [MNB*21] as well as to compare forces acting on the inner and outer vessel wall [MVB*17b]. With this, clear differences could be detected between healthy volunteers and patients with an aortic valve defect.

2.2. Comparative Visualizations on the Wall

Side-by-side views with simplified geometric representation can also be used to compare wall-related data. Goubergrits et al. [GSK*12] generated disc-shaped representations of aneurysms which are arranged side by side to compare stress distributions. Meuschke et al. [MGB*18] used scatter plot matrices to compare simulated scalar values defined on aneurysm vessel walls. Meuschke et al. [MGW*18] also presented an automatic computation of morphological aneurysm descriptors, which was later used in an automatic aneurysm detection approach [LMW*19] to compare these descriptors between multiple aneurysms.

In addition, abstract 2D visualizations of the spatial domain created according to a standard anatomy-driven subdivision scheme simplify the comparison tasks. Inspired by the cardiac *Bull's Eye Plot (BEP)*, Köhler et al. [KMP*15] designed an abstract 2D plot of the spatial aortic domain to compare measured blood flow information between patients. The aortic centerline is mapped to the plot's radius, where the angle encodes the measured time steps. The plot area color-codes a scalar value related to vortical flow. Meuschke et al. [MKP*16] extended this plot by discretizing the radius into four segments based on four anatomical parts of the aorta to encode the spatio-temporal development of vortices.

2.3. Comparative Visualizations for Lumen and Wall

For the comparative analysis of wall and flow features, glyphs are well suited. Van Pelt et al. [vPGL*14] designed a comparative visualization of qualitative flow features comprising *inflow jet* and *impingement zone* [GLvP*12] as well as quantitative WSS values for aneurysm treatment options. The user can investigate the untreated case and up to four virtual stenting configurations. The *inflow jet* and the *impingement zone* are represented by arrow glyphs and surface contours, respectively, and their color encodes the configuration ID. In addition, surface glyphs, called *flower glyphs*, are evenly distributed over the surface and show the temporal WSS behavior for different configurations over the cardiac cycle. The main disadvantages are the limited number (maximum five) of time steps considered and the dependency of the glyph sampling.

Conclusion. While existing visualizations for nasal flow [ZMH*09, XSZ*14] focus only on the analysis of single data sets, comparative methods for blood flow data are limited to specific components of the underlying data. In addition, these approaches show significant simplifications, such as a limitation to a few time steps that can be investigated or a reduced representation of the flow volume in the form of streamlines. In contrast, our system allows a comprehensive visual comparison of the whole spatio/temporal 3D domain including vessel/mucous wall, flow lumen/cavity and path lines.

3. Requirement Analysis

We discussed the comparative visual analysis of simulated flow data with two CFD experts, interested in vascular pathologies and simulation of nasal aerodynamics, to identify requirements. Their goal is to better understand factors that lead to the progression of diseases. Moreover, they want to investigate how different treatment methods influence the forces acting on the vessel/mucous wall as well as on the internal flow and how the relation between wall and flow characteristics is changed. Based on Amar et al. [AES05], who defined ten typical analysis tasks, we discussed their approach to compare two data sets and difficulties encountered. Except for the sorting task, all analytical tasks, comprising retrieving value, filtering, finding extremum, computing derived values, determining value ranges, characterizing distributions, cluster flow patterns, finding anomalies, and determine correlations between scalar fields, currently play a role in the comparative exploration of medical flow data.

Currently, our experts use the commercial software *Ansys Ensight* for the comparative analysis of simulated flow data. Ensight is a specialized post-processing software with which multiple data sets can be loaded side by side. Typically, a scalar field is color-coded inside the flow volume or on the 3D surface mesh. The experts search manually for scalar field characteristics that differ between the data sets as well as correlations that might be an indicator for disease progression or treatment success. Animations are used to display the data over time. Color-coded cut planes are manually placed within the flow volumes to investigate characteristics. While the cameras are linked between views, cut planes are not automatically synchronized. The experts described the activation of linking options as very troublesome due to the large feature set of Ensight. They also pointed out that analyzing scalar fields just on a 3D representation is cumbersome, since they have to rotate and zoom in 3D to explore the whole domain. Moreover, there is no option to compare qualitative flow patterns which would be helpful to assess, e.g., treatment success.

The experts wished a system that enables fast and simple visual comparison of medical flow data regarding the analytical tasks. Since the experts often have a mental model of interesting scalar field values, efficient filter techniques are needed to direct the experts' attention to such regions. Moreover, visualizations are needed that give a spatial overview about scalar fields and techniques that allow a visual comparison of flow patterns. In addition, the storage of findings for upcoming explorations and discussions should be supported. Based on these discussions and an analysis of the state of the art, we summarize the requirements for COMFIS as follows:

R. 1: Provide an overview visualization showing the distribution of a scalar field defined on one of the input components.

R. 2: A simplified representation of morphology is needed to easily investigate morphological and flow-related changes.

R. 3: Provide visualization and interaction concepts to highlight interesting regions within the flow volume.

R. 4: Provide a comparative visualization to analyze multiple scalar attributes simultaneously.

R. 5: Landmarks should be set in different regions and time steps, whereby an individual label can be assigned.
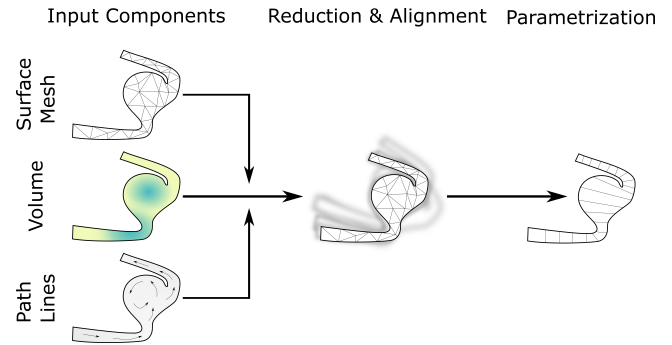

Figure 1: *Data pre-processing in COMFIS. Two data sets are loaded, comprising a surface mesh, volume, and path lines, respectively. Before the comparative analysis starts, the high-resolution components of both data sets are reduced, aligned, and parameterized.*

R. 6: Provide an option to easily formulate more advanced data processing queries that should be applied to selected components.

4. Comparative Analysis of Medical Flow Data

This section describes the functionality of COMFIS w.r.t. to the requirements and analytical tasks. As input, two data sets are expected that describe two states of a flow simulation, such as before and after treatment. Each data set comprises up to three major components:

- A surface mesh representing the morphology of the considered anatomical wall region. It consists of vertices and triangles.
- A volume representing the flow domain that consists of tetrahedra.
- Path lines representing qualitative flow patterns inside the volume.

All primitives, i.e., surface vertices, path line points, and tetrahedrons inherit multiple time-dependent scalar fields, such as flow velocity, pressure or wall shear stress (WSS). Note that our tool does not assume that all these three components are available. For example, it would be possible that no path lines are present.

COMFIS is written in c++17 and employs OpenGL 4.5 for rendering. We used the third party libraries: imGui for the user interface, implot to generate 2D plots, such as scatterplots and correlation matrices, GLEW for OpenGL extensions, and Eigen for solving equation systems. No commercial or GPL libraries are used. Platform dependencies are avoided. We recommend a quad core CPU and 16 Gb RAM to be able to load larger simulated data sets and to handle the high computational effort during pre-processing. Further implementation details are given in the upcoming subsections.

4.1. General Workflow of COMFIS

We provide a *comparative workflow*, where domain experts can analyze data sets collaboratively. The collaboration is realized by user-defined landmarks that can be analyzed by other experts. After loading, some pre-processing steps are performed, see Fig. 1. First, we reduce the very memory-intensive simulated flow data, see Sec. 4.2. Next, we align and parameterize both data sets to generate comparative visualizations. Both, the data set alignment and parameterization, are described in Sec. 4.3. After pre-processing, the comparative visual analysis can take place.

We decided to arrange both data sets side by side, as this is a familiar view for the domain experts. Moreover, we use a horizontal split as default, since vessels and nasal structures are mostly elongated. However, the user can manually switch the splitting direction. On the surface mesh, a selected scalar field is encoded using a yellow-to-dark-purple color scale. Similarly, the Viridis color scale is used to encode a scalar field on the path lines or to visualize the volume data based on direct volume rendering. Based on various selection menus, the user can decide which component to display or create integrated visualizations, such as the path lines within the surface mesh. Here the user can choose whether the front faces of the surrounding geometry are removed or displayed transparently. Furthermore, the user can determine which analysis task should be executed. Depending on the selected task, suitable visualizations are activated, see Sec. 4.4. Showing all visualizations at once would result in an overloaded user interface, with many representations visible that would not be helpful for all tasks, see Sec. 4.5.

The goal was to combine visualization techniques, the experts are familiar with, such as scatter plots and volume rendering. Another key design decision involved the analysis of flow information over time. We discussed with our experts whether visualizations that allow a detailed comparison of scalar fields between both data sets over time are needed. The basis for this was the *skyline visualization* of Meuschke et al. [MVG*21] which allows to study multiple scalar fields over time defined on a 3D surface. While this already results in complex representations consisting of multiple linked views, a comparative analysis of scalar fields over time for two data sets would be more complex. Furthermore, the experts stated that the analysis over time plays a subordinate role, since usually they are interested in selected time points, such as systole in blood flow data. Therefore the focus of this work is not on the simultaneous analysis of several time steps, but the comparative analysis of all components at selected time steps. We use animated visualizations to provide an overview about the temporal behavior. The user can pause and restart the animation, and switch to any time step.

4.2. Volume Reduction

The volume of simulated flow data may amount to several gigabytes per time step, which hampers an efficient comparative analysis with interactive frame rates. According to our experts, these high resolutions are unnecessary to investigate hot spots in the volume, i.e., regions with very high and low scalar values. Therefore, we reduce the size of the flow volume while preserving hot spots.

For reducing the flow volume, we employed the fast method by Hu et al. [HZG*18] that generates a high-quality tetrahedral mesh without inversions or self-intersections and with 70% fewer tetrahedra on average. After reduction, we have to transfer the time-dependent scalar fields of the original volume V_o to the reduced volume V_r. Thus, for each vertex inside V_r the corresponding scalar values of the vertices of V_o need to be determined. For this purpose, we iterate over the tetrahedra of V_r and determine all vertices of V_o that are inside the current tetrahedron of V_r, see Fig. 2. Afterwards, we assign each of these vertices to one of the vertices of the current tetrahedron of V_r based on the Euclidean distance, similar to a Voronoi decomposition inside the tetrahedron. Then, we iterate over all vertices of the current tetrahedron of V_r. For each vertex v_i, we
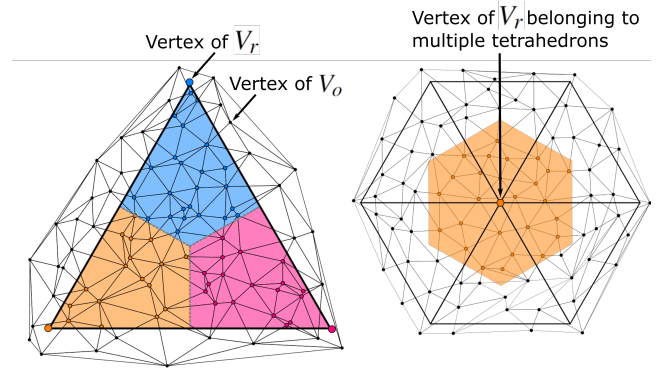

Figure 2: *Reducing the original volume V_o. Left: For each tetrahedron of the reduced volume V_r, the vertices of V_o lying within it are assigned to a vertex of V_r represented by the color-coded segments. For all assigned vertices, the minimum or maximum value of each scalar field is assigned to the corresponding vertex of V_r. Right: this is repeated for all vertices of V_r, where a vertex (e.g., large orange vertex in the center) might belong to multiple tetrahedrons. In this case, the list of corresponding vertices of V_o (all vertices in the orange region) is extended.*

determine the minimum or maximum value (decided by the user) of the corresponding scalar values and assign it to v_i. As default, we use the maximum value similar to Meuschke et al. [MGB*18]. This assignment is repeated for every scalar field and for every time step.

4.3. Alignment and Parameterization

After volume reduction, we have to ensure that both data sets are aligned. The alignment of data sets is the prerequisite for computing a consistent parameterization along all three components, which is necessary for many tasks, e.g., comparing flow patterns, see Sec. 4.4. However, data sets, representing different scenarios, e.g., vessel structures before and after treatment, are usually not aligned.

For aligning two data sets, we employ the commonly used *iterative closest point* (ICP) algorithm [Zha94], which was successfully applied to medical flow data [MOJB*19]. In the next step, we compute a parameterization along the u-component of the (u,v) parameterization space for three main components, called u-parameterization. There are many parameterization techniques to generate 2D simplified representations of 3D vascular structures, such as whole vessel trees [LL19], cerebral aneurysms [MVG*21], or aortic diseases [MGB*18]. However, existing methods have two disadvantages. First, they are not designed to generate a suitable parameterization on volume data or path lines, where in some cases also the parameterization of large spherical structures, such as aneurysms, is very limited [LL19]. Second, these methods require the determination of computationally intensive geometric properties, such as curvature information, geodesics, skeleton, or root point. Moreover, in many approaches a cut line needs to be defined to open the mesh, which influences strongly the shape of the resulting 2D representation [KMM*18]. Therefore, we present a simplified technique, which yields a good u-parameterization along all three components (also for spherical structure) within a few seconds.
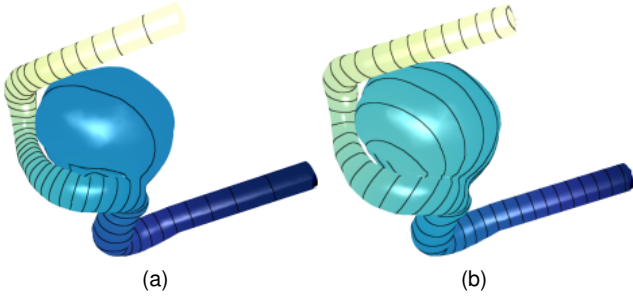
Figure 3: *Parameterization of an aneurysm with the Fiedler vector. In (a) the Fiedler vector is shown, whereas in (b) the Poisson equation was solved to obtain an evenly spread parameterization.*

First, we compute a u-parameterization along the surface mesh. For this, we use the Fiedler vector $\mathbf{u}_F = (u_1, \ldots, u_n)$, which is the eigenvector of the Laplacian matrix $\mathbf{L} \in \mathbb{R}^{n \times n}$ with the smallest non-zero eigenvalue [IL05]. An alternate definition is [Lev06]:

$$\text{Minimize: } F(\mathbf{u}_f) = \mathbf{u}_F^T \mathbf{L} \mathbf{u}_F = \sum_{i,j} w_{i,j}(u_i - u_j)^2$$
$$\text{Subject to: } \sum_i u_i = 0 \text{ and } \sum_i u_i^2 = 1. \tag{1}$$

The rational behind this is that the Fiedler eigenvector gives a natural ordering of the mesh vertices. When color-coding the Fiedler eigenvector on the surface, the isolines are spread irregularly, see Fig. 3(a). Therefore, we additionally ensure a regular spread along the parameterization by solving the Poisson equation:

$$\mathbf{L}\mathbf{u} = \nabla \cdot (\nabla \mathbf{u}_F)/\|\nabla \mathbf{u}_F\|, \tag{2}$$

This yields an evenly spread u-parameterization, see Fig. 3(b). By normalizing the gradient, we ensure that the parameter $\mathbf{u}$ moves consistently with uniform speed along the surface.

To generate a coherent volume parameterization, we apply the idea of *image completion* [CGJ*15]. Here, a missing part in an image can be complemented by solving the Laplace equation with Dirichlet boundary condition. We consider the volume as the missing part that needs to be filled and the surface mesh as the boundary. To solve the Laplace equation, we use the tetrahedral Laplacian $\mathbf{L}_V$ [Jac13]. We assume that the m vertices of the tetrahedral are ordered such that the last l vertices represent the boundary vertices, i.e., the surface mesh and the first k vertices represent the interior vertices, i.e., the volume. This assumption is not generally valid and only serves to simplify the following equation, which must be solved:

$$\left(\frac{\mathbf{L}_V|_{m \times k}}{\mathbf{0} \mid \mathbf{I}_{l \times l}} \right) \mathbf{u}_F = \begin{pmatrix} 0 \\ \vdots \\ 0 \\ \mathbf{u}. \end{pmatrix} \tag{3}$$

Here, $\mathbf{I}$ represents the identity matrix, $\mathbf{0}$ the matrix with zeros, and $\mathbf{L}_V|_{m \times k}$ the tetrahedral Laplacian of the interior vertices. Solving this equation yields the parameterization $\mathbf{u}_F$ for the volume.

To generate a parameterization of the path lines, we determine for every vertex on a path line in which tetrahedron it is lying. Next,
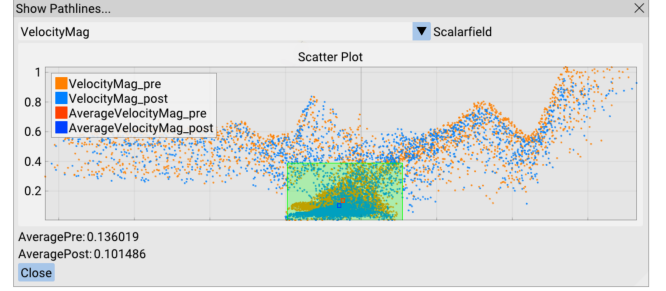

Figure 4: *Spatialized scatter plot showing the distribution of a scalar field along a component. On the $x-$axis, the spatial location of the component is encoded, where the scalar values are encoded on the $y-$axis. Here, the velocity magnitude along the path lines is encoded for the aneurysm data set, before and after treatment.*

we compute the barycentric coordinates of the path line vertex and apply these to the $\mathbf{u}_F$ values of the tetrahedron vertices to yield a parameterization for each path line point.

Next, we determine the parameterization on the second aligned data set. For each vertex, we determine in which tetrahedron of the first data set it lies. Afterwards, we compute the barycentric coordinates and determine the u-parameterization, similar to the the path lines. For vertices that are not within a tetrahedron, the nearest projection onto the surface is determined. Since the projection lies inside a surface triangle, we can again determine the u-parameterization with barycentric coordinates.

4.4. Comparative Features

We provide six comparative features to accomplish the derived analytical tasks. These features allow to analyze scalar fields on the walls and inside the flow volume. A comparison of vector fields is not integrated, as this was not assessed as necessary by the domain experts. Each feature is automatically applied to both data sets.

Spatialized scatter plots. To provide an overview of a selected scalar field (meet **R. 1**) along one of the input components, we decided to use scatter plots which are frequently used to assess the correlation of attributes [KH12]. In contrast to traditional scatter plots, which encode two attributes, in COMFIS only one selected scalar field is considered within a scatter plot, see Fig. 4. We used the second plot axis to encode a spatial direction along the considered component. Thus, the $x-$axis of the scatter plot shows the u-parameter of the parameterization, and the y-axis represents the values of a selected scalar field at the current time step. The scalar values are represented by circles colored to the corresponding data set. Additionally, a rectangular region can be defined to show the average values of both data sets within this region.

Contour view. Since morphological changes are hard to investigate in 3D due to occlusion problems, we provide a 2D slice view, which shows the wall extent of both data sets comparatively (meet **R. 2**). The contour view provides the cross-section of the surface along the u-parameterization, see Fig. 8. With this, the user can detect surface regions where both data sets strongly differ. In 3D, the position of the current cross-section is highlighted by a colored surface
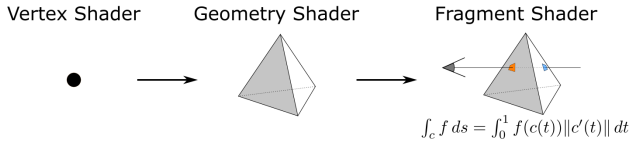
Figure 5: *Computation of the step size-independent DVR.*

contour. The intersection can be moved along the surface mesh and the contour view is updated accordingly. Within the contour view, also the corresponding volume data can be color-coded. In addition, the experts mentioned that they would like to see whether the flow moves forward or backward through the plane, since backflow is an indication of abnormal flow behavior. Therefore, the path lines can also be visualized as animated particles within the contour view. Whenever they pass the contour view, the intersection point is displayed, with particles of both data sets being represented by different colors. Light reddish or blueish particles move forward and dark reddish or blueish particles move backward.

Volume rendering. Direct volume rendering (DVR) typically uses a fixed step size for ray casting. However, if the step size is not chosen optimally, primitives within volume are skipped and thus interesting values not being represented. While in structured volume grids twice the underlying resolution is used as step size, specifying a minimum step size in unstructured grids leads to a high computational effort. Therefore, we provide a DVR that does not depend on the step size, see Fig. 5. For this purpose, we provide the midpoint of every tetrahedron in the vertex shader, passing it to the geometry shader. In that stage, every midpoint knows the surrounding vertices that build the corresponding tetrahedron. This allows us to create a triangular strip that gives the surface of the tetrahedron. In the fragment shader, we obtain the current fragment position and the view direction of the camera to determine which of the tetrahedron triangles the ray intersects. This yields two intersection points $\mathbf{p}_1, \mathbf{p}_2 \in \mathbb{R}^3$ and its corresponding triangles. Using the barycentric coordinates, we can also determine the value of the scalar field $f(\mathbf{p}_1), f(\mathbf{p}_2)$ by linear interpolation of the scalar values of the triangle vertices. Then, we calculate the line integral inside the tetrahedron, which is simply the difference of the interpolated scalar values multiplied with the length of the intersection points:

$$\int_c f\, ds = \int_0^1 f(c(t))\|c'(t)\|\, dt = \int_0^1 f(\mathbf{p}_1 + t(\mathbf{p}_2 - \mathbf{p}_1))\|\mathbf{p}_2 - \mathbf{p}_1\|\, dt$$
$$= \frac{1}{2} \cdot \frac{f(\mathbf{p}_2) - f(\mathbf{p}_1)}{\|\mathbf{p}_2 - \mathbf{p}_1\|}.$$

Note, that we linearized the scalar field inside the tetrahedron. The values are then blended by using OpenGL's function *glBlendFunc(GL_ONE, GL_ONE)* with *glBlendEquation(GL_FUNC_ADD)*. The blended values are used to color the fragment in a second render pass. Furthermore, instead of determining the line integral inside the tetrahedron, the maximal occurred value of the scalar field of both intersection points can be employed to generate a maximum intensity projection (MIP), see Fig. 6. In this case, OpenGL's blending function is set to *GL_MAX*. The user can decide which rendering method to use.
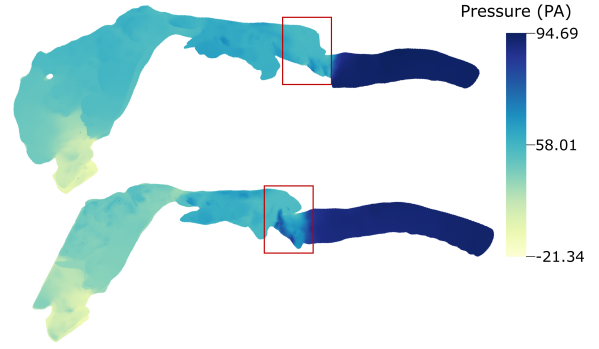

Figure 6: *Comparative MIP rendering showing pressure values in the larynx data set before (top) and after treatment (bottom). Strongly differences occur near the vocal folds.*

In case of the line integral, the user can adapt the transfer function to highlight volume regions with suspicious scalar values in both data sets (meet **R. 3**). For this purpose, we provide an interactive histogram showing the distribution of the currently visualized scalar field. The histogram is drawn for both data sets where the color and opacity values of the bins can be adapted.

Due to the time-dependent data, the histogram changes over time. Therefore, we compute the histogram on the fly by using OpenGL's atomic counter. We discretized the values of the current scalar field into bins and whenever a scalar value falls into a certain bin, the atomic counter is increased. For the determination of the bin number k we employ the widely used Sturges' formula [Stu26]: $k = \lfloor \log_2(n) \rfloor + 1$, with n being the number of scalar values. If the bin number exceeds the maximum allowed number of atomic counter buffers, we set the number of bins to this maximum buffer number.

Slice-based view. Besides showing the data sets side-by-side, we provide a slice-based view to directly encode scalar fields of both data sets on one of the three components, see Fig. 7. The basic idea is to divide the current component into slices, where on each slice a specific scalar field can be encoded. This facilitates the simultaneous comparison of multiple scalar fields between data sets (meet **R. 4**).

First, the user has to select which scalar fields should be considered for the slice-based view as well as in which order. The current component is cut into slices along the *u*-parameterization, with a user-defined slice thickness. The defined order of the scalar fields is then mapped to the slices, which repeats until the last slice is reached. Fig. 7 shows an example of the slice-based view for each component. For example, the pressure on the surface mesh (top sub figure) of both data sets can be analyzed simultaneously.

Listing 1: *Lua example to find the vertex with highest pressure.*

```lua
function getValue()
   if (pressure1>result or firstCall) then
      result=pressure1
      bestVertexId=currentVertexId
   end
   return result, bestVertexId
end
```
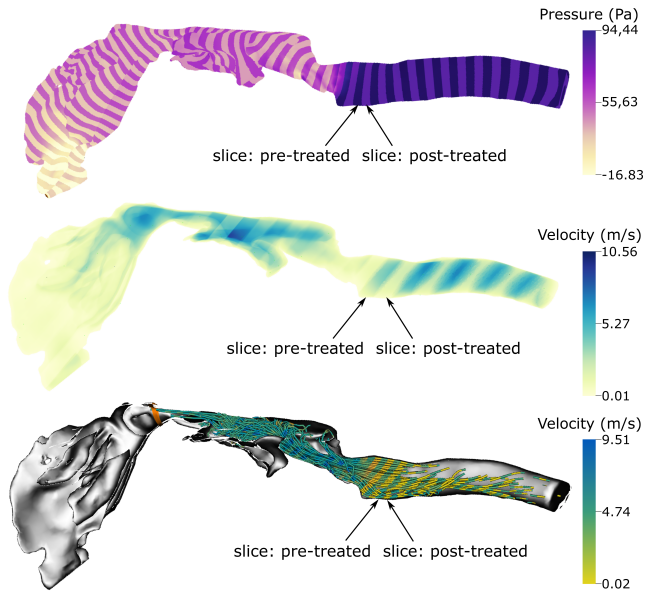
Figure 7: *Slice-based view to compare scalar fields of both data sets directly on one component: surface mesh (top), volume (middle), or path lines (bottom). Here, pressure and velocity values are compared before and after surgical treatment of laryngeal cancer.*

Landmarks. The domain expert may identify interesting regions that should either be further explored or shown to another expert. Therefore, landmarks in form of circles with a description can be added to the data (meet **R. 5**). The user can load previously set landmarks. By selecting a landmark, the camera moves to the corresponding spatio-temporal position by applying all visualization settings that were active during its definition.

Individual data processing. To handle more specific processing tasks, we offered the possibility to program individual queries (meet **R. 6**). For this purpose, we integrated the script language *Lua* (https://www.lua.org/). The user can implement a function that runs over all vertices of a selected component and compares their scalar values with the script. It is possible, e.g., to determine the global maximum of a scalar field and the corresponding vertex position in both data sets, see List. 1. The camera is moved automatically to the determined vertex.

4.5. Low-Level Analytic Tasks

In the following, we explain how the nine analytical tasks are supported for the three input components within COMFIS.

Retrieve values. To get the concrete scalar values at a specific position, the user can define a circular region of individual size and position on one of the three components. We determine for both data sets, the vertices and corresponding scalar values of the current component that lie within the screen space circle. Afterwards, all retrieved values are visualized using the spatialized scatter plot. Thus, regional values can be compared between the data sets.

Moreover, the scatter plot can also be used to **compute derived values**, e.g., mean and median scalar values over time within a

selected region as well as to **determine ranges of scalar values**. Here, also the scripting functionalities of Lua can be used to process any other statistical measure. In addition, the mean and standard deviation is shown for both configurations in the scatter plot to **characterize the distribution**.

Filter. Similar to Meuschke et al. [MVB*17a], the user can select multiple scalar fields on the surface or the path lines as well as ranges to determine conspicuous regions w.r.t. multiple scalar fields. Only regions that fulfill the defined criteria are color-coded in both data sets. Filtering within the volume can be achieved by adapting the transfer function of the DVR.

Find extremum. COMFIS analyzes the current component, e.g., the surface mesh for both data sets, to find vertices with high and low scalar values. The user is asked to define the size of the neighborhood, which determines the size of the region that is used for searching local extremes. Per default, we set it to one, using the 1-ring neighborhood around each vertex as search space. Increasing the size of the neighborhood results in fewer extremes until only the global minimum or maximum is detected. At the end, we list all extremes of both data sets in a table. By clicking on a table entry, the camera moves to the corresponding vertex position showing the extrema. This task is also provided for the volume and the path lines.

Cluster. To detect qualitative flow patterns, we integrated the path line clustering by Meuschke et al. [MVPL18]. The method refers to the spatio-temporal behavior of path lines to obtain compact and temporally coherent clusters. Within a cluster, the path lines follow a similar direction and occur at similar time points.

The clustering is performed for both data sets individually. To allow an efficient comparison of the cluster results between the data sets, we have to determine corresponding clusters. For this purpose, we determined a representative for each cluster. Following the recommendation by Oeltze et al. [OLK*14], we used *density-based representatives* [OWG09] to well represent the clusters' shape. First, a Cartesian grid around the cluster is created, using its axis-aligned bounding box. The resolution of the grid corresponds to the resolution of the image data used to reconstruct the surface mesh. Next, a density value is determined for each grid cell, which corresponds to the number of passing lines. The density values are mapped to the associated path line points and integrated along each line. The line with the highest value is used as representative.

To explore the cluster results, the user can select a cluster in one of the two data sets. Based on the cluster representative, the most similar representative is detected in the second data set. This similarity computation is based on the mean distances of path lines [MVPL18], the measure that was also used for the path line clustering. The representative with the smallest mean distances to the selected representative is used as corresponding representative (cluster).

Find anomalies. Anomalies refer to nearby regions of the surface mesh or volume, where strongly varying scalar values occur. To identify such regions, the slice-based view can be used. In the case of a thin thickness, the slices are spatially very close to each other which allows a comparative study of anatomical regions, such as the aneurysm dome, w.r.t. scalar changes. For a more detailed quantitative analysis of such regions, the scatter plot can be used.

Correlation. Analyzing multiple scalar fields w.r.t. correlations may reveal that a scalar field may be left out for further analysis. For this purpose, we provide a correlation matrix. Again, the user can decide for which component the correlation matrix should be displayed. Afterwards, for every vertex, the scalar values are used to determine the Pearson's coefficient which is color-coded in the corresponding matrix entry. The correlation matrix can be animated to show the temporal behavior of scalar field correlations.

5. Evaluation

We conducted a qualitative evaluation with five domain experts to assess the suitability of COMFIS. The experts were three CFD experts (E1, E2, E3) dealing with hemodynamic and aerodynamic simulations (3, 7, and 14 years of experience), and two radiologists (E4, E5) with 26 and 15 years of experience, respectively. We used two use cases, a simulated cerebral aneurysm data set before and after treatment as well as a simulated nasal aerodynamics data set of a patient with laryngeal cancer. At the beginning of each session we presented all functionalities of our tool for about 15 min. Then, each expert could choose one of the two data sets they wanted to analyze. While E4, E5, and two of the CFD experts (E1, E3), wanted to analyze the aneurysm data set, E2 explored the laryngeal data set. We briefly discussed with each expert the tasks to be performed to avoid misunderstandings w.r.t. task definition. Then, each expert spent about 25 min analyzing the selected data set considering the tasks. We documented which features were used to complete the tasks, which problems were encountered, and which results the experts arrived at using the *think aloud* method. The evaluation was performed on a standard desktop computer with an Intel Core i5 with 2.8 GHz, 16 GB RAM, and an NVidia GeForce GTX 1080 Ti. For all presented models we achieve a real-time performance of approximately 40 *FPS* after pre-processing. This performance test was conducted with a resolution of 2560×1440 pixels.

Cerebral hemodynamics use case. Cerebral aneurysms – pathological bulges of brain arteries – carry the risk of rupture and causing stroke. Since aneurysm treatment carries risks for the patient, clinical research aims to reliably distinguish rupture-prone and harmless aneurysms as well as to determine an optimal treatment. In combination with morphological descriptors, such as aneurysm size and location, hemodynamic aneurysm modeling is used to investigate the interaction between blood flow and aneurysm initiation, growth, and rupture risk [DCM*18]. For the selection of an appropriate treatment method, clinical researchers are interested in analyzing the flow characteristics before and after treatment. Therefore, implant placement is simulated. The resulting flow attributes and patterns provide valuable information about intra-aneurysmal flow [MTXS14].

We reconstruct vascular surface meshes from contrast-enhanced CT images of the aneurysm morphology [MNP11]. A virtual stent is implanted in the vessel to prevent blood flow in the aneurysm. For this purpose, the fast stent deployment approach by Berg et al. [BDJ17] was used, simulating different treatment scenarios. CFD simulations are performed before and after implant placement using the solver *STAR-CCM+ 11*. Path lines are emitted at the cross-sectional area where the fluid enters the solid domain with an adaptive fifth order Runge-Kutta method. Further details regarding the simulation and post-processing can be found in [BRB*15].

Nasal aerodynamics use case. The airways are essential for both the breathing process and verbal communication. Diseases and malformations can significantly affect both and make medical treatment necessary. Computational methods enable the investigation and evaluation of diseases or treatment scenarios [MEP13, BCC*16].

A concrete medical use case for CFD simulations within the respiratory tract is to find an optimal treatment strategy in case of laryngeal cancer. We used a head-neck-CT data set with laryngeal cancer to analyze nasal aerodynamics. A laryngeal resection was performed, removing the epiglottis and parts of the vestibular folds. A surface mesh of the airway lumen before and after surgery is generated using a threshold-based segmentation. We consider the process of exhalation from the lower trachea to the nasal opening. A volume flow rate of 27.5 l/min is assumed, which corresponds to regular breathing intensity. The fluid dynamics are described by the Navier-Stokes equations, which are solved using *STAR-CCM+ 13.02*. Finally, instantaneous pressure and velocity fields are exported and path lines are integrated. Further details regarding the simulation and post-processing can be found in [VAJ19, VVS*22].

5.1. Task-based Expert Evaluation

We performed a task-based evaluation to check whether COMFIS allows an efficient comparative analysis of medical flow data and fulfills all defined requirements. For each of the more general tasks (cf. Sec. 3), we came up with specific example tasks (ET) that were designed together with the two experts who were interviewed during the requirement analysis but did not participate in the evaluation. The following tasks should be performed by the users:

ET 1: Retrieve value. Compare the values of a selected scalar field at the same position of both surface meshes.

ET 2: Filter. Find a spatio-temporal region inside the flow volume of both data sets where a selected scalar field shows high values.

ET 3: Find extremum Find extreme scalar values, which can be considered as outliers, within a spatio-temporal region in one data set and assess if these outliers exist also in the second data set.

ET 4: Compute derived value. Compare the mean values of a scalar field within a volume slice at a specific time step between both data sets.

ET 5: Determine range. Compare both data sets w.r.t. the range of a selected scalar field within a spatio-temporal region on the path lines.

ET 6: Characterize distribution. Compare both data sets w.r.t. the standard deviation of a scalar field within a spatio-temporal surface region.

ET 7: Cluster. Compare two corresponding flow patterns between both data sets regarding flow complexity.

ET 8: Find anomalies. Determine adjacent surface regions that differ strongly between the two data sets w.r.t. a selected scalar field.

ET 9: Correlate. Compare a spatio-temporal region on the surface mesh of both data sets w.r.t. correlations between two scalar fields.
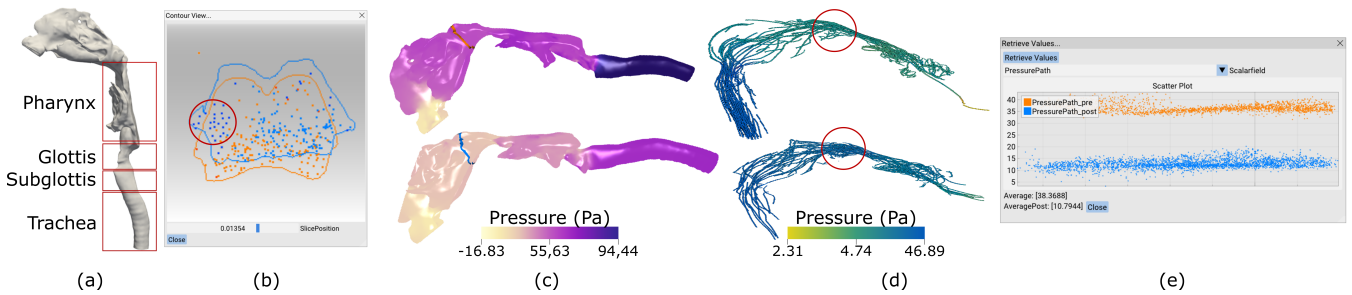
Figure 8: *Comparative analysis of the laryngeal data set. The contour view (b) shows increased back flow after surgery (bluish particles) near the pharyngeal entrance (a), while the pressure on the surface (c) and on the path lines (e) was reduced after surgery (bottom row). Related to the backflow, a post-treated cluster reveals a vortex, which does not exist in the pre-treated data.*

5.2. Results of the Task-based Expert Evaluation

In the following, we summarize the experts' feedback during the study as well as occurring problems.

ET 1. To compare values of an individual scalar field on the vessel or mucous wall, the experts initially just used the color-encoding on the surface meshes. However, the numerical differences may be quite small, so color coding is not well suited. Therefore, CFD experts in particular have resorted to the suggested circular region to retrieve the values. They have chosen a very small radius to compare values at specific positions on the surface. The resulting scatter plot easily allowed the scalar values to be compared.

ET 2. All experts confirmed that the MIP rendering immediately shows regions with high or low values. Moreover, the adaption of the histogram allows an efficient filtering of volume regions that fulfill specific criteria. Especially the radiologists rated the interactive histogram as an easy way to narrow down volume data to areas of interest. Besides the comparison of one scalar field, E1 and E2 were interested in filtering multiple scalar fields. While this is easily possible for the surface and the path lines using the slider-based filtering, more cognitive effort is needed for the volume.

ET 3. To find extrema, all experts initially used the spatialized scatter plot. While the scatter plot can in principle be used for this task, it requires manual effort to compare the scalar values in different regions. Therefore, we suggested to use the automatic search of extrema based on the neighborhood size to be specified. In principle, this feature combined with the approach of moving the camera to the associated 3D position was found to be very helpful. However, there were problems in choosing a suitable neighborhood size. While a maximum size to find the global maximum was understandable for the experts, a size of one can lead to many extrema. The experts had difficulties to find a suitable value between one and the maximum number of vertices to get an explorable number of extrema. In the future, this should be supported by, for example, diagrams that give indications of where extrema are located.

ET 4. The spatialized scatter plot is useful for various comparative tasks. E2 selected a slice within the volume near the pharyngeal entrance to investigate mean pressure values before and after surgery, see Fig. 8. It was observed that the mean pressure after treatment is lower, which could indicate that the lungs are better supplied with air. To confirm this insight, the contour plot was activated, where

however, E2 observed that also the amount of back flow seems to be increased (red circle in the contour view in Fig. 8(b)). Since backflow indicates vortical flow, the user also compared flow patterns and found that in the region of the set contour view a vortex is visible after treatment that was not there in the pre-treated data (red circles on the path lines in Fig. 8(d)). Such vortices could have a negative effect on the voice. Such findings were described as important to better understand and assess surgery outcome.

ET 5. In addition, using the spatialized scatter plot the experts were able to compare ranges of a selected scalar field within a surface region. One exemplary result is depicted in Fig. 4. Here, E5 used the scatter plot to depict the magnitude of the flow velocity along the path lines within the aneurysm before and after treatment. E5 selected the part of the scatter plot (green box) that corresponds to the aneurysm part of the 3D vascular model. It can be observed that the inserted implant reduces the flow velocity inside the aneurysm as desired, thus reducing the risk of rupture.

ET 6. Similarly, the experts explore the distribution of a scalar field on the surface using the spatialized scatter plot. Here, they mentioned that the statistical analysis of subregions within the scatter plot is more interesting than showing the statistical measures over the whole parameterization. Usually, experts are interested in specific parts of the whole flow domain, such as the aneurysm or the glottis (area of the larynx where the vocal cords are located). Here, the scatter plot helps to investigate whether there are increases or decreases in mean flow or pressure, as well as to assess the dispersion of values, which may either indicate treatment success or failures.

ET 7. While the radiologists were less familiar with qualitative flow patterns, the CFD experts emphasized the added value of the flow pattern exploration, since tools used so far are not able to detect and compare qualitative flow patterns. With COMFIS, changes of the flow patterns could be detected. While the aneurysm data before treatment show strong vortical flow patterns inside the aneurysm, corresponding flow patterns after stenting show a strongly reduced vortical behavior, which is an indication of successful treatment.

ET 8. To determine adjacent regions on the surface mesh that differ between the data sets, the radiologists initially used the side-by-side view. However, a comparison of neighboring regions is rather difficult, because they always have to switch between both views to find regions. Therefore, we suggested to use the slice-based view. While they initially found this view confusing, after a few minutes

they familiarized with it. They explored different layer thicknesses and scalar fields, where they found neighboring regions that had vastly different values. In contrast, the CFD experts used directly the slice-based view having lesser understanding problems due their experience in the evaluation of volume data by setting cut planes, which is similar to the concept of the slice-based view. However, the slice-based view applied to the path lines remained confusing to the experts due to occlusion problems and complex stripe patterns.

ET 9. To analyze correlations between scalar fields, the experts used the correlation matrices of both data sets side by side. In case of the aneurysm data, E3 explored the behavior of WSS and pressure. The expert assumed an increased rupture risk for surface regions with high pressure and WSS values. While the correlation matrices show no clear linear correlations between these scalar fields, there are regions in the pre-treated data with high pressure and WSS. Moreover, E3, observed that these values were strongly reduced after treatment, which indicates a positive treatment outcome.

6. Discussion

The evaluation indicates that COMFIS allows an efficient comparative analysis of two simulated medical flow data sets. In contrast to commercial software, which require scripting skills to generate comparative visualizations, COMFIS is tailored to the requirements of domain experts. To not overwhelm domain experts, we combine and extend familiar visualization concepts, such as scatter plots, DVR, cut planes, and path line representations. The complexity of the visualizations can be adjusted interactively, e.g., by first selecting the contour plot and then activating the path lines to explore the degree of backflow. Next, the path lines clusters could be activated to explore quantitative flow patterns. Thus, the user is not confronted with complex representations right from the start, which can lead to excessive demands.

COMFIS could also be used to analyze measured blood flow data (4D PC-MRI). Data sets of healthy probands could be compared to better understand the variability of normal blood flow as well as pre- and post treated data to investigate whether treatment leads to a normalization of the blood flow behavior. However, 4D PC-MRI data usually require different pre-processing steps to reduce imaging artifacts. For pre-processing, the freely available tool *Bloodline* [KGGP19] can be used, which exports the three components (surface mesh, volume, and path lines) we deal with.

Limitations. The results of the path line clustering depend on the seeding strategy. We used a standard seeding technique in our work. A more detailed investigation how different seedings influence the clustering results as well as a comparative analysis of alignment algorithms would be interesting points for future work, but are not the focus of this paper.

In addition, we used Sturges' formula (recall Sec. 4.4) to generate the histogram. However, it expects a normally distributed input which cannot be guaranteed in our cases. The influence on the resulting histogram depending on the distribution of the scalar field would have to be examined and how this changes the volume rendering. Moreover, the spatialized scatterplot preserves structural information only along one main direction. Since COMFIS was developed for the analysis of flow data obtained in elongated vessels or nasal

structures, this is not a fundamental limitation. In the case that complex structural variations along the y-axis occur, these would not be represented in the spatialized scatterplot.

In principle, an arbitrary number of scalar fields can be compared in adjacent regions using the slice view. The evaluation showed that a simultaneous analysis of more than two scalar fields lead to complex visualizations that require a lot of attention. Moreover, COMFIS can be used to compare any two selected data sets. However, data sets with very different topologies can lead to registration errors, which then result in representations that are difficult to interpret. Therefore, we recommend to use COMFIS for the comparison of different configurations of a data set, e.g., before and after treatment. Nevertheless, a robustness analysis of the parameterization as well as comparisons with existing parameterization methods [LL19, MGB∗18] will be necessary in the future. In particular, possibilities should be given to improve the parameterization with semi-automatic methods in case of errors in the mapping.

Improvements. An improvement would be to provide multiple spatialized scatter plots to compare multiple scalar fields simultaneously. In addition, more automatic methods to find interesting characteristics, e.g., detection of strong vortical flow or regions where two scalar fields strongly correlate, would further improve the comparative analysis. Similarly, the user should be guided towards selecting an interesting contour view, where, e.g., both data sets strongly differ. While the CFD experts considered the Lua scripting as a helpful addition to explore more mathematical quantities, a set of pre-defined scripts should be integrated, which can be activated on demand or serve as a template for own adaptions.

7. Conclusion and Future Work

We presented COMFIS, a visualization system to compare two simulated medical flow data sets. For the design of COMFIS, we discuss tasks and requirements with domain experts. Several features support the comparative analysis of the three main components: surface mesh, flow volume, and path lines. Based on simulated data sets from medical applications, interesting differences between data sets could be observed, which can provide insights on the progression and appropriate treatment of vascular and respiratory diseases. Thus, all participating experts confirmed that COMFIS was usable to compare complex medical flow data and that they would employ it for future explorations of other data sets.

For future work, we would like to further support the documentation of findings by generating reports from the findings the experts made during the analysis. Moreover, we would like to extend COMFIS regarding the comparative analysis of multiple data sets, such as ensemble simulations. Therefore, powerful options to compare more than two data sets would be needed. In addition, techniques should be developed and evaluated that allow a direct time-dependent comparison of volume data. Moreover, a larger user study with more data sets from different applications as well as alternative visualizations would be necessary to further evaluate the suitability of COMFIS.

References

[AES05] AMAR R., EAGAN J., STASKO J.: Low-level components of analytic activity in information visualization. In *Proc. of IEEE Symposium on Information Visualization* (11 2005), pp. 111– 17. 3

[AH11] ANGELELLI P., HAUSER H.: Straightening tubular flow for side-by-side visualization. *IEEE Trans. Vis. Comput. Graph. 17*, 12 (2011), 2063–70. 2

[ALEK15] ANDERSSON M., LANTZ J., EBBERS T., KARLSSON M.: Quantitative assessment of turbulence and flow eccentricity in an aortic coarctation: impact of virtual interventions. *Cardiovascular engineering and technology 6*, 3 (2015), 281–93. 2

[BCC*16] BATES A., COMERFORD A., CETTO R., SCHROTER R., TOLLEY N., DOORLY D.: Power loss mechanisms in pathological tracheas. *Journal of biomechanics 49*, 11 (2016), 2187–92. 8

[BDJ17] BERG P., DARÓCZY L., JANIGA G.: Virtual stenting for intracranial aneurysms: A risk-free, patient-specific treatment planning support for neuroradiologists and neurosurgeons. In *Computing and Visualization for Intravascular Imaging and Computer-Assisted Stenting*. 2017, pp. 371–411. 8

[BEGP18] BEHRENDT B., EBEL S., GUTBERLET M., PREIM B.: A framework for visual comparison of 4d pc-mri aortic blood flow data. In *Proc. of Eurographics Workshop on Visual Computing for Biology and Medicine* (2018). 2

[BPEGP21] BEHRENDT B., PLEUSS-ENGELHARDT D., GUTBERLET M., PREIM B.: 2.5D geometric mapping of aortic blood flow data for cohort visualization. In *Proc. of Eurographics Workshop on Visual Computing for Biology and Medicine* (2021). 2

[BRB*15] BERG P., ROLOFF C., BEUING O., VOSS S., SUGIYAMA S.-I., ARISTOKLEOUS N., ANAYIOTOS A. S., ASHTON N., REVELL A., BRESSLOFF N. W., ET AL.: The computational fluid dynamics rupture challenge 2013 – Phase II: variability of hemodynamic simulations in two intracranial aneurysms. *J Biomech Eng 137*, 12 (2015), 121008. 8

[CGJ*15] COHEN-OR D., GREIF C., JU T., MITRA N. J., ZHANG H. R.: *A Sampler of Useful Computational Tools for Applied Geometry, Computer Graphics, and Image Processing*. CRC Press, 2015. 5

[DCM*18] DETMER F. J., CHUNG B. J., MUT F., SLAWSKI M., HAMZEI-SICHANI F., PUTMAN C., JIMÉNEZ C., CEBRAL J. R.: Development and internal validation of an aneurysm rupture probability model based on patient characteristics and aneurysm location, morphology, and hemodynamics. *Int. Journal of Computer Assisted Radiology and Surgery 13*, 11 (2018), 1767–79. 1, 8

[dHvPJV14] DE HOON N., VAN PELT R., JALBA A., VILANOVA A.: 4D MRI Flow Coupled to Physics-Based Fluid Simulation for Blood-Flow Visualization. *Comput Graph Forum 33*, 3 (2014), 121–30. 2

[EDK*20] EBEL S., DUFKE J., KÖHLER B., PREIM B., BEHRENDT B., RIEKENA B., JUNG B., STEHNING C., KROPF S., GROTHOFF M., ET AL.: Automated Quantitative Extraction and Analysis of 4D flow Patterns in the Ascending Aorta: An intraindividual comparison at 1.5 T and 3 T. *Scientific reports 10*, 1 (2020), 1–13. 1

[GAW*11] GLEICHER M., ALBERS D., WALKER R., JUSUFI I., HANSEN C. D., ROBERTS J. C.: Visual comparison for information visualization. *Information Visualization 10*, 4 (2011), 289–309. 2

[GBMK07] GARCIA G. J. M., BAILIE N., MARTINS D. A., KIMBELL J. S.: Atrophic rhinitis: a CFD study of air conditioning in the nasal cavity. *J Appl Physiol 103* (2007), 1082–92. 8

[GFL*20] GUO R., FUJIWARA T., LI Y., LIMA K. M., SEN S., TRAN N. K., MA K.-L.: Comparative visual analytics for assessing medical records with sequence embedding. *Visual Informatics 4*, 2 (2020), 72–85. 1

[Gle17] GLEICHER M.: Considerations for visualizing comparison. *IEEE Trans Vis Comput Graph 24*, 1 (2017), 413–23. 2

[GLvP*12] GASTEIGER R., LEHMANN D. J., VAN PELT R., JANIGA G., BEUING O., VILANOVA A., THEISEL H., PREIM B.: Automatic Detection and Visualization of Qualitative Hemodynamic Characteristics in Cerebral Aneurysms. *IEEE Trans Vis Comput Graph 18*, 12 (2012), 2178–87. 2

[GSK*12] GOUBERGRITS L., SCHALLER J., KERTZSCHER U., VAN DEN BRUCK N., PÖTHKOW K., PETZ C., HEGE H.-C., SPULER A.: Statistical wall shear stress maps of ruptured and unruptured middle cerebral artery aneurysms. *J R Soc Interface 9*, 69 (2012), 677–88. 1, 2

[GTB*10] GOUBERGRITS L., THAMSEN B., BERTHE A., POETHKE J., KERTZSCHER U., AFFELD K., PETZ C., HEGE H.-C., HOCH H., SPULER A.: In vitro study of near-wall flow in a cerebral aneurysm model with and without coils. *Am J Neuroradiol 31*, 8 (2010), 1521–28. 1, 2

[HZG*18] HU Y., ZHOU Q., GAO X., JACOBSON A., ZORIN D., PANOZZO D.: Tetrahedral meshing in the wild. *ACM Trans Graph 37*, 4 (2018), 1–14. 4

[IL05] ISENBURG M., LINDSTROM P.: Streaming meshes. In *Proc. of IEEE Visualization* (2005), pp. 231–38. 5

[Jac13] JACOBSON A.: *Algorithms and interfaces for real-time deformation of 2d and 3d shapes*. PhD thesis, ETH Zurich, 2013. 5

[JĆS*20] JANOVIĆ N., ĆOĆIĆ A., STAMENIĆ M., JANOVIĆ A., DJURIĆ M.: Side asymmetry in nasal resistance correlate with nasal obstruction severity in patients with septal deformities: Computational fluid dynamics study. *Clinical Otolaryngology 45*, 5 (2020), 718–24. 1

[KGGP19] KÖHLER B., GROTHOFF M., GUTBERLET M., PREIM B.: Bloodline: A system for the guided analysis of cardiac 4d pc-mri data. *Computers & Graphics 82* (2019), 32–43. 1, 10

[KH12] KEHRER J., HAUSER H.: Visualization and visual analysis of multifaceted scientific data: A survey. *IEEE Trans Vis Comput Graph 19*, 3 (2012), 495–513. 5

[KKN*19] KARIMKESHTEH S., KAUFHOLD L., NORDMEYER S., JARMATZ L., HARLOFF A., HENNEMUTH A.: Comparing subjects with reference populations-a visualization toolkit for the analysis of aortic anatomy and pressure distribution. In *Int. Conf. on Functional Imaging and Modeling of the Heart* (2019), pp. 370–78. 2

[KMM*18] KREISER J., MEUSCHKE M., MISTELBAUER G., PREIM B., ROPINSKI T.: A survey of flattening-based medical visualization techniques. In *Comput Graph Forum* (2018), vol. 37, pp. 597–624. 4

[KMP*15] KÖHLER B., MEUSCHKE M., PREIM U., FISCHBACH K., GUTBERLET M., PREIM B.: Two-Dimensional Plot Visualization of Aortic Vortex Flow in Cardiac 4D PC-MRI Data. In *Proc. of BVM* (2015), pp. 257–261. 2

[LAM*12] LARRABIDE I., AGUILAR M. L., MORALES H. G., GEERS A. J., KULCSÁR Z., RÜFENACHT D., FRANGI A. F.: Intra-Aneurysmal Pressure and Flow Changes Induced by Flow Diverters: Relation to Aneurysm Size and Shape. *Am J Neuroradiol 34*, 4 (2012), 816–22. 2

[Lev06] LEVY B.: Laplace-beltrami eigenfunctions towards an algorithm that "understands" geometry. In *Proc. of the IEEE International Conference on Shape Modeling and Applications* (USA, 2006), p. 13. 5

[LL19] LICHTENBERG N., LAWONN K.: Parameterization, feature extraction and binary encoding for the visualization of tree-like structures. *Comput Graph Forum 39*, 1 (2019), 497–510. 4, 10

[LMW*19] LAWONN K., MEUSCHKE M., WICKENHÖFER R., PREIM B., HILDEBRANDT K.: A geometric optimization approach for the detection and segmentation of multiple aneurysms. In *Comput Graph Forum* (2019), vol. 38, pp. 413–25. 2

[LPK*14] LAMATA P., PITCHER A., KRITTIAN S., NORDSLETTEN D., BISSELL M. M., CASSAR T., BARKER A. J., MARKL M., NEUBAUER S., SMITH N. P.: Aortic relative pressure components derived from four-dimensional flow cardiovascular magnetic resonance. *Magnetic Resonance in Medicine 72*, 4 (2014), 1162–69. 2

[MEP13] MITTAL R., ERATH B. D., PLESNIAK M. W.: Fluid dynamics of human phonation and speech. *Annual review of fluid mechanics 45* (2013), 437–67. 8

[MGB*18] MEUSCHKE M., GÜNTHER T., BERG P., WICKENHÖFER R., PREIM B., LAWONN K.: Visual Analysis of Aneurysm Data using Statistical Graphics. *IEEE Trans Vis Comput Graph 25*, 1 (2018), 997–1007. 1, 2, 4, 10

[MGW*18] MEUSCHKE M., GÜNTHER T., WICKENHÖFER R., GROSS M., PREIM B., LAWONN K.: Management of cerebral aneurysm descriptors based on an automatic ostium extraction. *IEEE Comput Graph Appl 38*, 3 (2018), 58–72. 2

[MKP*16] MEUSCHKE M., KÖHLER B., PREIM U., PREIM B., LAWONN K.: Semi-automatic Vortex Flow Classification in 4D PC-MRI Data of the Aorta. *Comput Graph Forum 35*, 3 (2016), 351–60. 2

[MLK*16] MEUSCHKE M., LAWONN K., KÖHLER B., PREIM U., PREIM B.: Clustering of aortic vortex flow in cardiac 4d pc-mri data. In *Bildverarbeitung für die Medizin*. Springer, 2016, pp. 182–87. 2

[MNB*21] MEUSCHKE M., NIEMANN U., BEHRENDT B., GUTBERLET M., PREIM B., LAWONN K.: Gucci-guided cardiac cohort investigation of blood flow data. *IEEE Trans Vis Comput Graph* (2021). 2

[MNP11] MÖNCH T., NEUGEBAUER M., PREIM B.: Optimization of vascular surface models for computational fluid dynamics and rapid prototyping. In *Workshop on Digital Engineering* (2011), pp. 16–23. 8

[MOJB*19] MEUSCHKE M., OELTZE-JAFRA S., BEUING O., PREIM B., LAWONN K.: Classification of Blood Flow Patterns in Cerebral Aneurysms. *IEEE Trans Vis Comput Graph 25*, 7 (2019), 2404–2418. 2, 4

[MSBM*22] MULLER-SIELAFF J., BELADI S. B., MEUSCHKE M., VREDE S., LUCAS P. J., PIJNENBORG J. M., OELTZE-JAFRA S.: Visual assistance in development and validation of bayesian networks for clinical decision support. *IEEE Trans Vis Comput Graph* (2022). 1

[MTXS14] MENG H., TUTINO V., XIANG J., SIDDIQUI A.: High wss or low wss? complex interactions of hemodynamics with intracranial aneurysm initiation, growth, and rupture: toward a unifying hypothesis. *American Journal of Neuroradiology 35*, 7 (2014), 1254–62. 1, 8

[MVB*17a] MEUSCHKE M., VOSS S., BEUING O., PREIM B., LAWONN K.: Combined Visualization of Vessel Deformation and Hemodynamics in Cerebral Aneurysms. *IEEE Trans Vis Comput Graph 23*, 1 (2017), 761–70. 7

[MVB*17b] MEUSCHKE M., VOSS S., BEUING O., PREIM B., LAWONN K.: Glyph-based comparative stress tensor visualization in cerebral aneurysms. In *Comput Graph Forum* (2017), vol. 36, pp. 99–108. 2

[MVG*21] MEUSCHKE M., VOSS S., GAIDZIK F., PREIM B., LAWONN K.: Skyscraper visualization of multiple time-dependent scalar fields on surfaces. *Computers & Graphics 99* (2021), 22–42. 4

[MVPL18] MEUSCHKE M., VOSS S., PREIM B., LAWONN K.: Exploration of blood flow patterns in cerebral aneurysms during the cardiac cycle. *Computers & Graphics 72* (2018), 12–25. 7

[NBR*18] NARATA A. P., BLASCO J., ROMAN L. S., MACHO J. M., FERNANDEZ H., MOYANO R. K., WINZENRIETH R., LARRABIDE I.: Early results in flow diverter sizing by computational simulation: quantification of size change and simulation error assessment. *Operative Neurosurgery 15*, 5 (2018), 557–66. 1

[OJMN*19] OELTZE-JAFRA S., MEUSCHKE M., NEUGEBAUER M., SAALFELD S., LAWONN K., JANIGA G., HEGE H.-C., ZACHOW S., PREIM B.: Generation and Visual Exploration of Medical Flow Data: Survey, Research Trends and Future Challenges. *Comput Graph Forum 38 (1)* (2019), 87–125. 1

[OLK*14] OELTZE S., LEHMANN D. J., KUHN A., JANIGA G., THEISEL H., PREIM B.: Blood Flow Clustering and Applications in Virtual Stenting of Intracranial Aneurysms. *IEEE Trans Vis Comput Graph 20*, 5 (2014), 686–701. 2, 7

[OWG09] O'DONNELL L. J., WESTIN C.-F., GOLBY A. J.: Tract-based morphometry for white matter group analysis. *Neuroimage 45(3)* (2009), 832–44. 7

[PP95] PAGENDARM H.-G., POST F. H.: *Comparative visualization: Approaches and examples*. Delft University of Technology Faculty of Technical Mathematics and Informatics, 1995. 1

[RvdHD*15] RAIDOU R. G., VAN DER HEIDE U. A., DINH C. V., GHOBADI G., KALLEHAUGE J. F., BREEUWER M., VILANOVA A.: Visual analytics for the exploration of tumor tissue characterization. In *Comput Graph Forum* (2015), vol. 34, pp. 11–20. 2

[SLG15] SU H., LOU W., GU J.: Clinical values of hemodynamics assessment by parametric color coding of digital subtraction angiography before and after endovascular therapy for critical limb ischaemia. *Chin Med J 95*, 37 (2015), 3036–40. 1

[Stu26] STURGES H. A.: The choice of a class interval. *Journal of the American Statistical Association 21*, 153 (1926), 65–6. 6

[VAJ19] VOSS S., ARENS C., JANIGA G.: Assessing transitional air flow during human exhalation from large eddy simulations based on spectral entropy. *Flow, Turbulence and Combustion 102*, 1 (2019), 117–28. 8

[VP04] VERMA V., PANG A.: Comparative flow visualization. *IEEE Trans Vis Comput Graph 10*, 6 (2004), 609–24. 2

[vPGL*14] VAN PELT R., GASTEIGER R., LAWONN K., MEUSCHKE M., PREIM B.: Comparative Blood Flow Visualization for Cerebral Aneurysm Treatment Assessment. *Comput Graph Forum 33*, 3 (2014), 131–40. 2

[VVS*22] VOSS S., VUTLAPALLI S. C., SAALFELD P., ARENS C., JANIGA G.: Cfd simulations of inhalation through a subject-specific human larynx–impact of the unilateral vocal fold immobility. *Computers in Biology and Medicine* (2022), 105243. 8

[XSZ*14] XI J., SI X., ZHOU Y., KIM J., BERLINSKI A.: Growth of nasal and laryngeal airways in children: implications in breathing and inhaled aerosol dynamics. *Respiratory Care 59*, 2 (2014), 263–73. 2

[Zha94] ZHANG Z.: Iterative point matching for registration of free-form curves and surfaces. *Int J Comput Vision 13*, 2 (oct 1994), 119–52. 4

[ZMH*09] ZACHOW S., MUIGG P., HILDEBRANDT T., DOLEISCH H., HEGE H.-C.: Visual exploration of nasal airflow. *IEEE Trans Vis Comput Graph 15*, 6 (2009), 1407–14. 2